ACS APPLIED ENERGY MATERIALS

www.acsaem.org Article

Influence of Oxygen Content on the Structural Evolution of SiO_x Thin-Film Electrodes with Subsequent Lithiation/Delithiation Cycles

Jung Hwi Cho,* Xingcheng Xiao, Mark W. Verbrugge, and Brian W. Sheldon*

Cite This: https://doi.org/10.1021/acsaem.2c01903 Read Online

ACCESS | Metrics & More | Article Recommendations | Supporting Information

ABSTRACT: SiO_x negative electrodes for Li-ion batteries enable high energy density while providing better structural integrity compared to pure Si electrodes. The oxygen content has a critical impact on structural changes that occur during electrochemical cycling. In this study, the near-surface structural evolution in SiO_x thin films with different compositions ($0.3 \leq x \leq 2$) was probed by various electrochemical techniques and X-ray photoelectron spectroscopy. These results show that all of the SiO_x films undergo significant chemical changes during cycling. Even the films with high oxygen content ($x = 2$) undergo significant restructuring after sufficiently long cycling times. The changes that occur in all films indicate that the near-surface regions of SiO_x materials react in ways that effectively make them part of the solid electrolyte interphase (SEI). This also implies that tuning the surface oxygen content of Si-based electrodes can be used to control SEI performance. Hence, the structural changes in SiO_x observed in this study may provide useful guidelines for designing passivating layers for improved cycle efficiency.

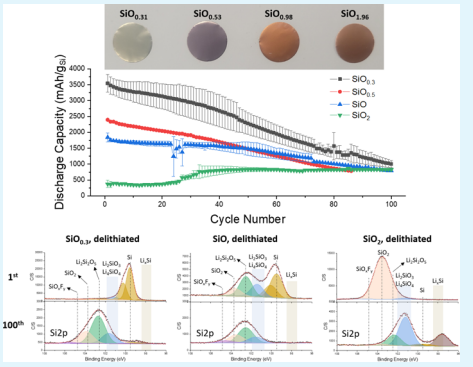

KEYWORDS: *lithium-ion batteries, SiO_x electrodes, oxygen content, thin film, structural change, electrochemistry, X-ray photoelectron spectroscopy*

1. INTRODUCTION

SiO_x electrodes for lithium-ion battery applications have been widely discussed in the research and engineering communities as they can enable higher energy densities (4000 to 1965 mA h/g for x ranging from 0 to 2, respectively).[1] In the present technology, small amounts of SiO_x in the coating or powder form are added to conventional graphite electrodes to boost capacity.[2,3] Some of the critical challenges associated with Si-based electrodes, such as large volume change degradation during lithium insertion/extraction, have limited the amounts of SiO_x to only a small fraction of the total active materials used in commercial products.[1] In order to fully realize the increased energy density from SiO_x materials, it is vital to evaluate the impact of the oxygen content in SiO_x on capacities and cycling stability. The structural changes in different SiO_x materials during lithiation and delithiation have been extensively investigated in recent years.[1,4−9] These studies largely show that increasing oxygen content enables higher cycling stability via the formation of various lithium silicates that suppress the volume change of electrochemically active Si species. The formation of additional oxygenated species (primarily lithium silicates and lithium oxide) is generally irreversible, and hence, this limits the amount of reversible capacity.[4−7,9] These investigations on structural changes in SiO_x materials have revealed many useful insights, but the effect of oxygen content on the corresponding structural evolution during longer-term cycling is not well understood. In general, successful commercial implementation requires structural stability over hundreds of cycles, and in SiO_x, this is a strong function of the oxygen content.

In this study, the effects of varying the SiO_x oxygen content on structural evolution over 100 cycles are investigated using thin-film electrodes. Compared to previous investigations, the thinner films (~50 nm) used in this study were designed to look more closely at changes in the material that occur closer to the surface. Electrochemical measurements using $dQdV$ analysis, hysteresis evolution, electrochemical impedance spectroscopy (EIS), and the chemical composition change probed by ex situ X-ray photoelectron spectroscopy (XPS) measurements reveal that the SiO_x structure evolves differently depending on the initial oxygen content.

2. EXPERIMENTAL SECTION

2.1. SiO_x Thin-Film Fabrication and Characterization. The SiO_x thin films were prepared by RF magnetron sputtering (Lesker PRO Line PVD Series) from a pure Si target (99.999%). 10 μm-thick Cu current collectors were used as the substrate. Before the

Received: June 16, 2022
Accepted: October 21, 2022

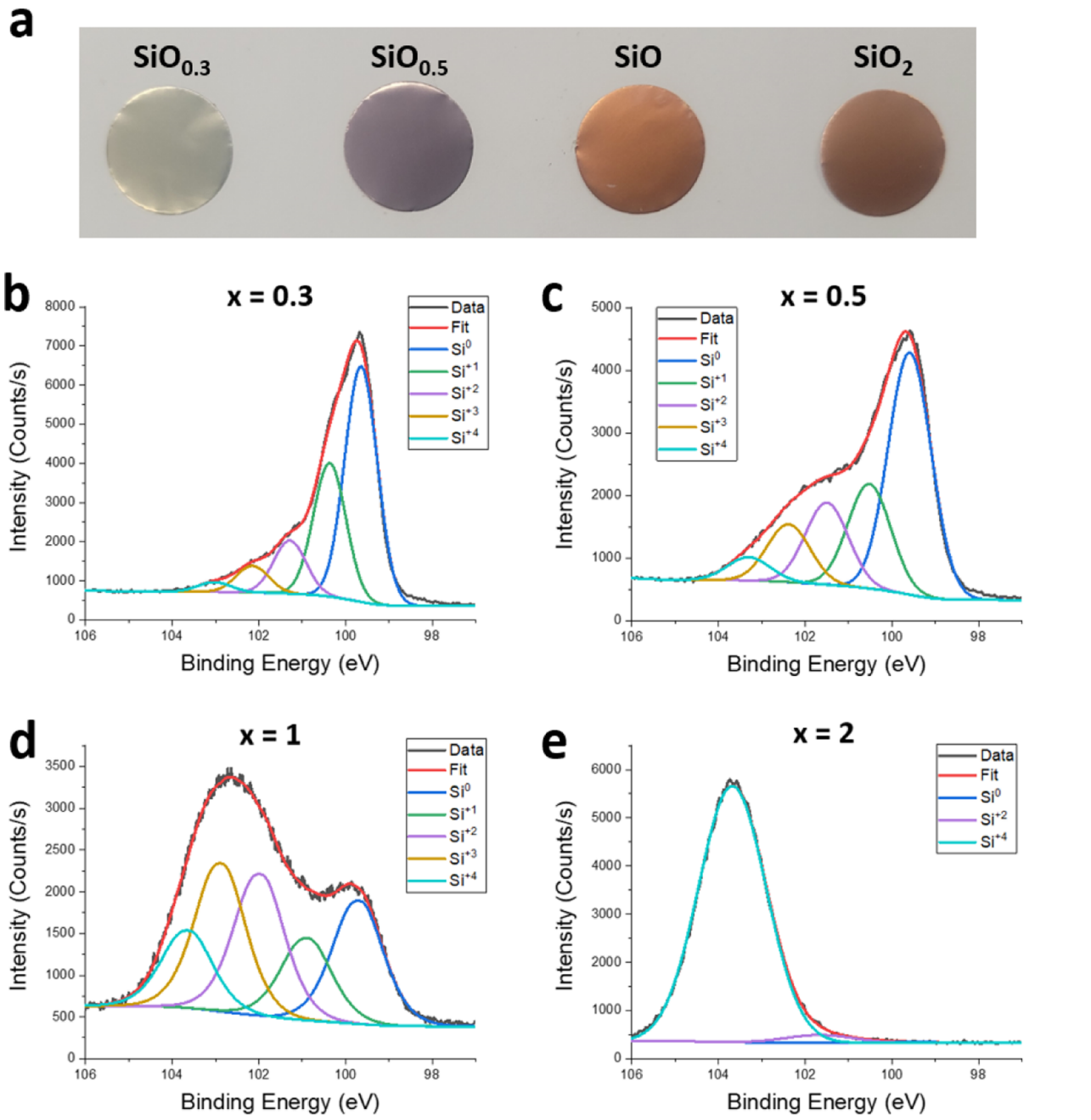

Figure 1. (a) Image of various compositions of the as-prepared SiO_x thin films on a Cu foil. XPS signals of Si 2p in four different 50 nm SiO_x thin films with compositions of (b) $SiO_{0.3}$, (c) $SiO_{0.5}$, (d) SiO, and (e) SiO_2 used in this study.

deposition, the chamber was allowed to pump down to ~7×10^{-7} mbar of chamber pressure. The amount of oxygen in the film was tuned by allowing various amounts of oxygen into the chamber prior to deposition. This was done by controlling the exposure time with a mixture of oxygen/argon (1:15 ratio), at a flow rate of 2 sccm. $SiO_{0.3}$, $SiO_{0.5}$, SiO, and SiO_2 films were created by allowing this mixture of gas to flow into the chamber for 0, 2, 8, and 15 min, respectively, prior to film deposition. The amount of Si used for each film was identical, corresponding to 50 nm of Si. The power used to sputter the Si target was 150 W, which corresponds to a deposition rate of 1.2 Å/s.

The chemical compositions of the as-created films were determined using XPS (Thermofisher K-Alpha). The spectra were collected with a pass energy of 12 eV and a step size of 0.05 eV, at a pressure of 2×10^{-8} mbar. Each film was etched with Ar-ion for 120 s prior to the measurement to remove any pre-existing oxide layer. The spectra were charge-corrected using the C−C bond present in the C 1s spectra at 284.8 eV. The spot size for the measurement was set at 200 μm. After the charge correction, the Si 2p spectra were then fitted with five peaks: Si^0, Si^{1+}, Si^{2+}, Si^{3+}, and Si^{4+} using a previously reported method to determine the oxygen content.[4,6,10]

2.2. Electrochemical Measurements. Fabricated films were punched out and assembled into coin cells in a half-cell configuration using a lithium foil as a reference electrode. Approximately 30 μL of 1 M $LiPF_6$ in an EC/DEC (1:2 v %) electrolyte was used for each coin cell. Constant-current-constant-voltage (CCCV) cycling was carried out for each film for 100 cycles at the rate of C/20, which was determined by the average discharge capacity during the first five cycles. The cutoff voltage was set at 25 mV and 1.5 V for lithiation and delithiation of the electrodes, respectively, with a 6 h hold at the end of each sequence. Cyclic voltammetry measurements were carried out with identically assembled coin cells, with a 0.01 mV/s scan rate and a 24 h hold on each end of the cutoff voltages (25 mV to 1.5 V).

https://doi.org/10.1021/acsaem.2c01903
ACS Appl. Energy Mater. XXXX, XXX, XXX−XXX

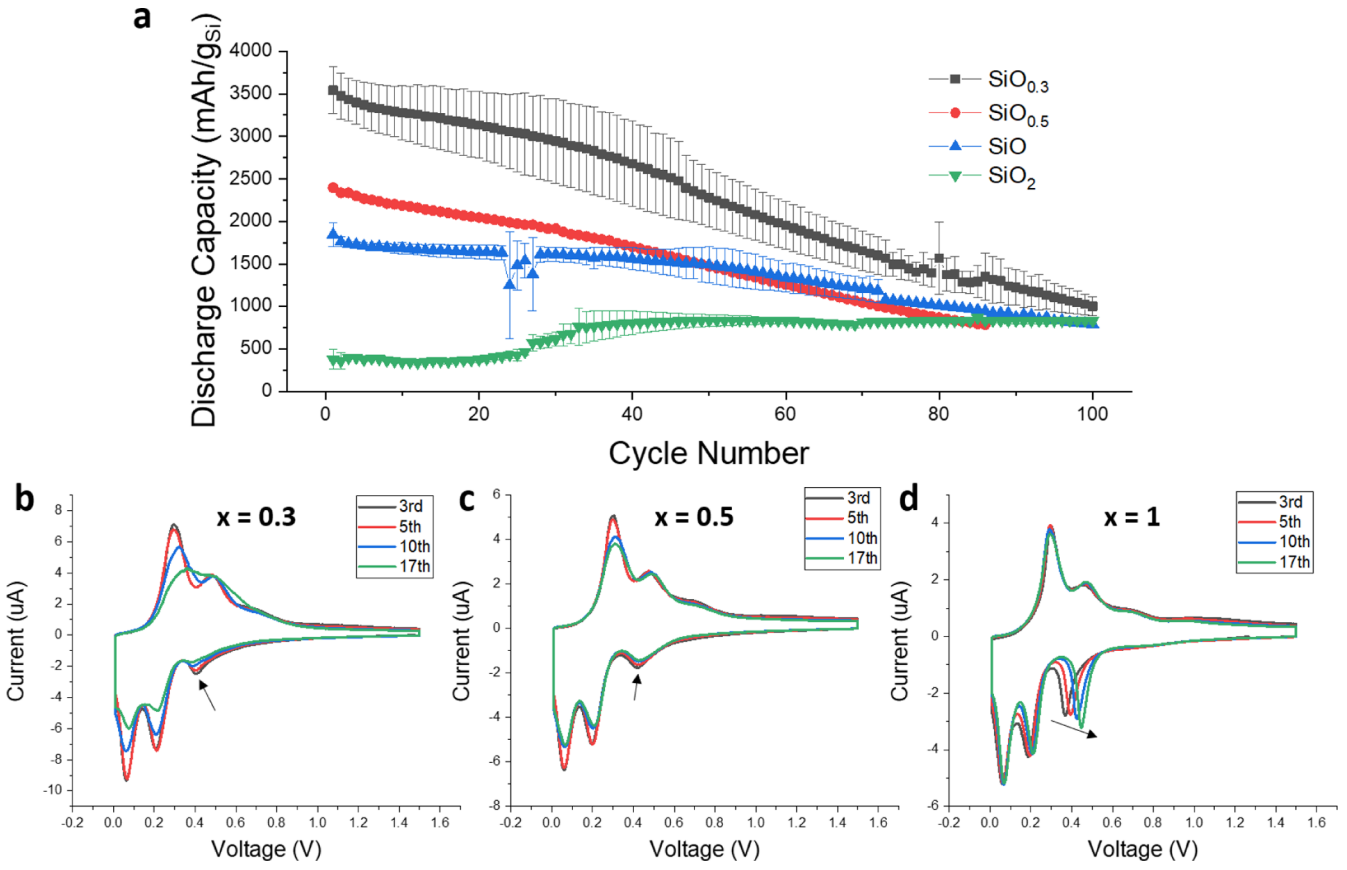

Figure 2. (a) Discharge capacity vs cycle number of various SiO_x thin film electrodes over 100 cycles. The electrodes are cycled via the CCCV protocol at full depth of discharge from 1.5−0.025 V with 6 hr holds at cutoff voltages. The current densities used here are approximately C/20 based on each of their respective capacities averaged from the first five cycles. The capacity values are given in mA h/g_{Si} based on the equal amount of pure Si deposited per film (50 nm in thickness). Two different cells were used here to verify the reproducibility, with the exception of $SiO_{0.5}$ film (b−d). Cyclic voltammograms of SiO_x thin film electrodes at 0.01 mV/s, starting at 1.5 V and scanning down to 25 mV with 24 hr holds at each end to ensure that the electrodes were fully lithiated/delithiated at the end of each sequence. The compositions of these films are $SiO_{0.3}$, $SiO_{0.5}$, and SiO, respectively.

EIS measurements were carried out every five cycles during the CCCV measurements after each lithiation and delithiation sequence. A resting time of 5 min was applied prior to each measurement. The frequency range was set at 100 mHz to 0.01 MHz with a 10 mV voltage amplitude.

2.3. dQdV Curves Using Diffcapanalyzer. To generate dQdV curves for all the CCCV measurements, a Python package called Diffcapanalyzer was utilized (developed by Thompson et al. from the University of Washington).[11] This tool allows facile and intuitive use to generate dQdV curves. The model provides a smoothing function by using a Savitzky−Golay filter and implements a pseudo-Voigt and Gaussian distribution for peak fitting. More details on this package can be found in ref 11.

2.4. XPS Measurements. After the electrochemical measurements, the coin cells were disassembled in an Ar-filled glovebox and the films were washed thoroughly using dimethyl carbonate (DMC). The samples were then transferred to XPS using a vacuum-sealed sample transfer holder. XPS measurements were performed using a Thermofisher K-Alpha X-ray photoelectron spectrometer system. The X-ray source was Al K-alpha. The irradiated spot size was set to 200 μm. Depth profiling was used to get spectra from the center of the film, which was determined by the onset of Cu peaks that indicate the bottom of the electrode. The etching current was at the "low" setting with 500 eV energy, with various etching times depending on the thickness of the films. A charge-neutralizing gun was used, and the additional charging was corrected by using the C−C bond present in the C 1s spectra at 284.8 eV, and also verified with Si 2p and O 1s literature values and by shifting the corresponding spectra. XPS fitting was conducted using Thermo Fisher's Avantage software (v 5.99).

2.5. Scanning Electron Microscopy Imaging. The film surfaces were examined by scanning electron microscopy (SEM) after disassembling the tested electrodes in an argon glovebox and thoroughly washing them with DMC (Aldrich). This was used to determine the morphology evolution of the film from pristine and after the 5th, 10th, 25th, 50th, and 100th cycles.

3. RESULTS AND DISCUSSION

3.1. Electrochemical Cycling and Evolution of Reaction Peaks Related to Oxygen Content. Four different SiO_x film materials prepared on a Cu foil using RF magnetron sputtering with a pure Si target are shown in Figure 1. The composition variations were controlled by varying the amounts of oxygen gas in the sputtering chamber prior to deposition[12] (see Section 2.1). All of these films contained an equivalent amount of Si (corresponding to 50 nm of Si mixed with various amounts of pre-existing oxygen). The top surface SEM image and the focused-ion beam cross-section of these films (Figure S1) show that the surfaces are all relatively smooth. The compositions were characterized by Si 2p XPS after etching of the top surface layer for the 30s and fit with five peaks: Si^0, Si^{1+}, Si^{2+}, Si^{3+}, and Si^{4+}.[4,6−8,10,13] Depth profiling was conducted to ensure compositional accuracy across their thicknesses, where minimal variations of x (no more than 0.02)

https://doi.org/10.1021/acsaem.2c01903
ACS Appl. Energy Mater. XXXX, XXX, XXX−XXX

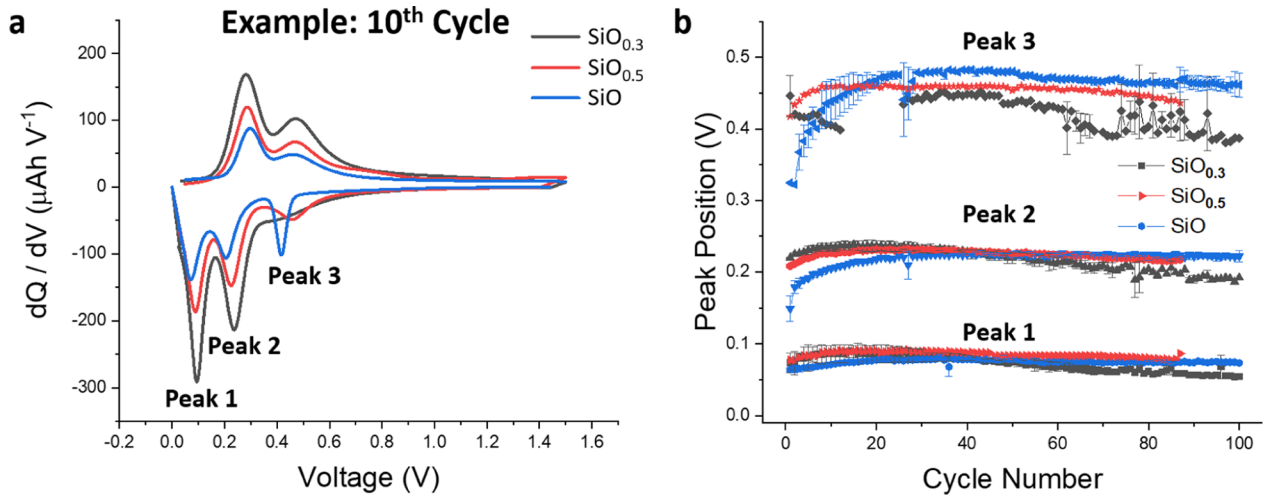

Figure 3. (a) dQdV curves of 10th cycle data for three SiO_x films with compositions of $SiO_{0.3}$ (black), $SiO_{0.5}$ (red), and SiO (blue) using Diffcapanalyzer.[11] Three main reaction peaks during lithiation are labeled peaks 1, 2, and 3, as shown in the plot. (b) Peak position vs cycle number for each respective reaction shown in Figure 2a.

were observed. The results in Figure 1b–e indicate that the compositions of these SiO_x films vary from x = 0.3 to x = 2.

The SiO_x films were punched out, assembled into a half-cell, and cycled between 25 mV to 1.5 V with 6 h holds at each cutoff voltage. The current density was set at C/20 based on the average discharge capacity of the first five cycles for each film. Discharge capacity versus cycle number is plotted in Figure 2a, which shows comparable trends based on the available literature data of SiO_x thin film electrodes that employ deep lithiation (≤25 mV), where higher capacity retention is observed with an increase in oxygen content but with lower reversible capacities.[5,7,8] Capacity retention per cycle can be improved by increasing the lithiation cutoff voltage to 75 mV as shown in Figure S2. As oxygen content increases, the capacity used per cycle decreases with increased capacity retention as expected. The SiO_2 film shows a significant increase in capacity around ∼30 cycles as cycling proceeds, which is distinctly different from that of the other films. The behavior of this highly oxygenated material will thus be discussed separately in Section 3.2 after considering the films with lower x.

The cyclic voltammograms of $SiO_{0.3}$, $SiO_{0.5}$, and SiO are plotted in Figure 2b–d, where a voltage scan rate at 0.01 mV/s was employed with the same voltage cutoffs as the CCCV cycles shown in Figure 2a. The two peaks below 0.3 V are the commonly observed two-phase reaction peaks with Si-rich electrodes that correspond to the formation of various a-Li_xSi and c-$Li_{15}Si_4$.[14−17] Compared to these peaks, however, the additional lithiation reaction peak near 0.4–0.5 V in Figure 2b–d shows changes that are relatively distinctive, further indicated by the arrows. The particular peak around 0.4–0.5 V has been previously attributed to the lithiation of oxygen-rich phases in SiO_x electrodes.[18] Figure S3 shows the overlapping third cycle CV plots of these films which show increased relative capacity utilization for the peak near 0.4–0.5 V as the oxygen content increases, suggesting that films that contain more oxygen result in the formation of higher concentrations of oxygen-related species such as lithium silicates during this reaction.

To further probe how the oxygen-related peak around 0.4–0.5 V evolves during cycling, dQdV plots were created with the same dataset used in Figure 2a. Figure 3a shows a representative 10th cycle dQdV plot for different SiO_x compositions. Lithiation is associated with peaks 1, 2, and 3, with peak 3 corresponding to the oxygen-related reaction at higher voltages (0.4–0.5 V) discussed above. Prior studies show that this peak is usually present only during the first 1–2 cycles as lithium silicate species form, and this peak is then generally regarded as irreversible.[5−8,18] However, this peak is present throughout 100 cycles in the current study (with the exception of $SiO_{0.3}$). In comparison with previous findings, the reason for the continuous detection of peak 3 throughout multiple cycles is unclear. However, a likely explanation is that the thinner films used here lead to different behaviors. Previous reports using amorphous SiO_x thin film electrodes (deposited with similar RF sputtering) showed that peak 3 did not appear after the first cycle for films with thickness in the micron range,[5,19] whereas films with 200 nm thickness exhibited peak 3 after the first cycle.[7] Thus, the results for the thinner SiO_x films used in the current study (Figure S1) suggest that the more extensive detection of the oxygen-related reaction at 0.4–0.5 V is enhanced with thinner electrodes.

Ex situ XPS data on $SiO_{0.5}$ before and after the evolution of this peak during the fifth cycle in Figure S4 show that the growth of the assigned $Li_2Si_2O_5$ peak is observed during this reaction. Previous studies using transmission electron microscopy and X-ray diffraction also reported that $Li_2Si_2O_5$ is the predominant reaction byproduct at potentials of 0.5 V during lithiation.[7,20] Subsequent formation and reduction of $Li_2Si_2O_5$ may explain the continuous observation of peak 3 throughout cycling in films with composition x > 0.3 as $Li_2Si_2O_5$ has been identified as one of the lithium silicate species and appears to be more reversible than other species such as Li_2SiO_3 and Li_4SiO_4.[7,21] In general, films that exhibit an amorphous nature result in the overlapping of peaks that correspond to similar chemical bonding states that are difficult to separate with peak-fitting software. Hence, it is also possible that other lithium silicate species may form during the peak 3 reaction during subsequent cycling[5] but that their growth was not distinctively observed via XPS.

Tracking the peak positions on dQdV plots for all 100 cycles readily shows that each of the lithiation peaks shifts over their

https://doi.org/10.1021/acsaem.2c01903
ACS Appl. Energy Mater. XXXX, XXX, XXX−XXX

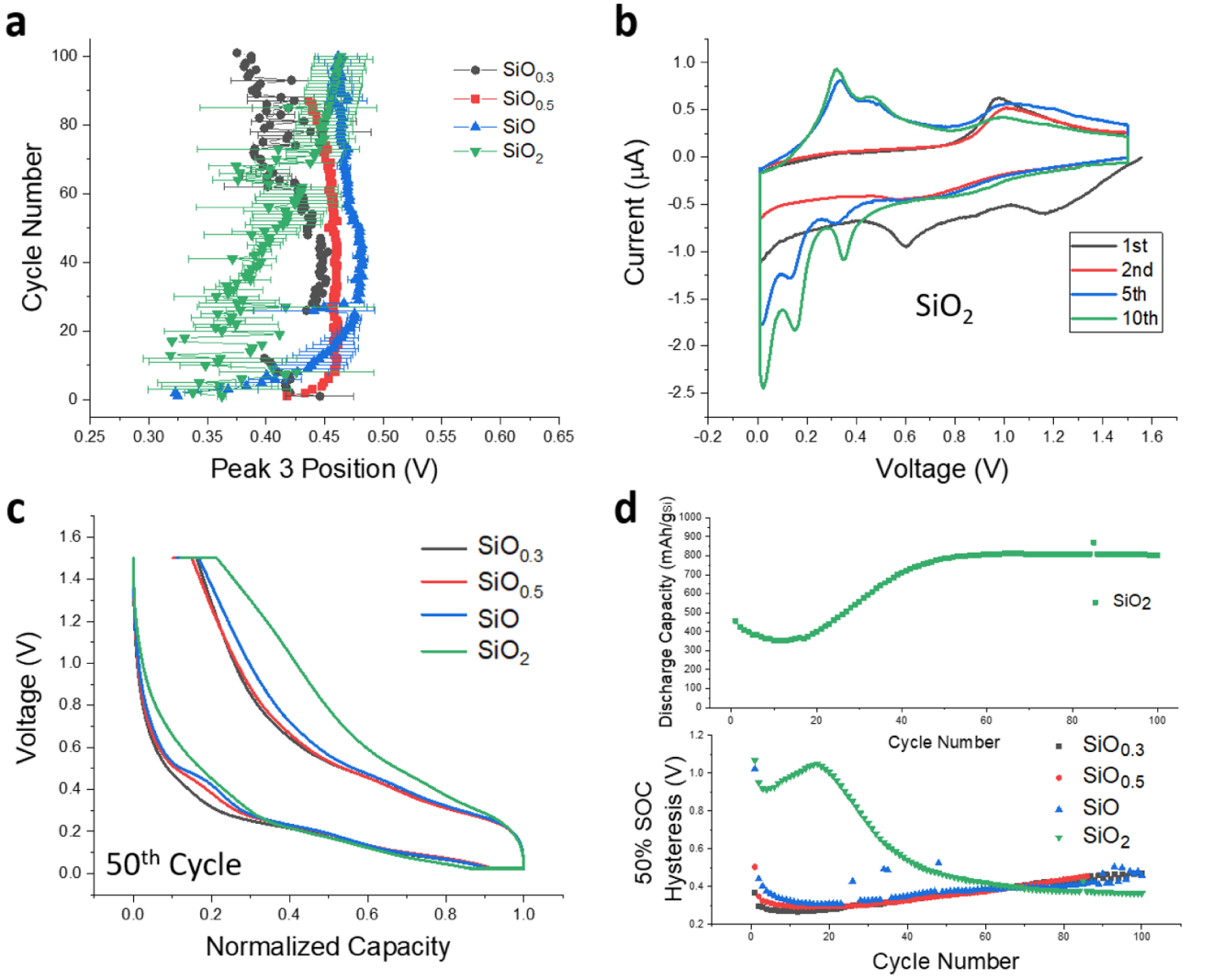

Figure 4. (a) Cycle number vs peak 3 positions (oxygen-related reactions). The figure is identical to the data shown in Figure 3b, except that the axes are flipped to observe the peak position shifts in a facile manner over 100 cycles. (b) Cyclic voltammograms of the SiO_2 film from the 1st−10th cycles. (c) Voltage vs normalized capacity of the 50th cycle of SiO_x films used in this study. (d) Discharge capacity of the SiO_2 film and voltage hysteresis at 50% SOC of various SiO_x films vs cycle number.

cycling history, as seen in Figure 3b. Peaks 1 and 2 correspond to the lithiation of Si-rich phases, both of which show similar peak-shift trends over the entire cycling history where the peak 1 and 2 positions do not vary significantly from each other with subsequent cycling. Compared to the relatively small shifts in the voltage positions for peaks 1 and 2, the oxygen-related peak 3 shows a more distinctive voltage shift that varies with the amount of oxygen present in the electrode films. As further indicated and supported by the arrows in the cyclic voltammogram in Figure 2b−d, the first few cycles show drastically different voltage shifting in Figure 3b. For example, for the $SiO_{0.3}$ film, peak 3 shifts to a lower voltage value for the first 12 cycles, while both more oxygenated samples of $SiO_{0.5}$ and SiO show a shift toward higher voltage during the first 10∼20 cycles. This unique voltage-shifting behavior of peak 3 for different films compared to the other Si-related reaction peaks indicates that the amount of oxygen present in the electrodes affects oxygen-related reaction evolution after subsequent cycling.

The peak shift observed in dQdV or CV measurements during cycling usually indicates both: (1) changes in impedance/resistance in bulk phases that are involved in the reaction, which relates to kinetic factors such as the surface overpotential and (2) structural changes that result from atomic rearrangements from bond breaking during lithium insertion/removal and possibly stress experienced by the bulk due to large volume changes. Note that all samples are cycled at C/20, so the contribution to the voltage shift by the overpotential is likely small. However, it is possible that structural change within the bulk of the electrode can facilitate or impede transport that is needed for a reaction to occur. Since the amount of Si−O affects its inherent electronic and ionic conductivities, the coupled effects of structural and impedance changes should also be considered.

3.2. Additional Cycling in the SiO_2 Material. Peak 3 shifting during electrochemical cycling in the SiO_2 electrodes is somewhat different. Figure 4a compares the peak 3 position evolution for films with different compositions, with the x and y axes flipped to better show the changes in the peak position (voltage). Figure 4a shows that for films with $x \leq 1$, the peak 3 position stabilizes after about ∼30 cycles. Previous findings on various SiO_x thin-film compositions $0.11 < x < 0.66$ show that

https://doi.org/10.1021/acsaem.2c01903
ACS Appl. Energy Mater. XXXX, XXX, XXX−XXX

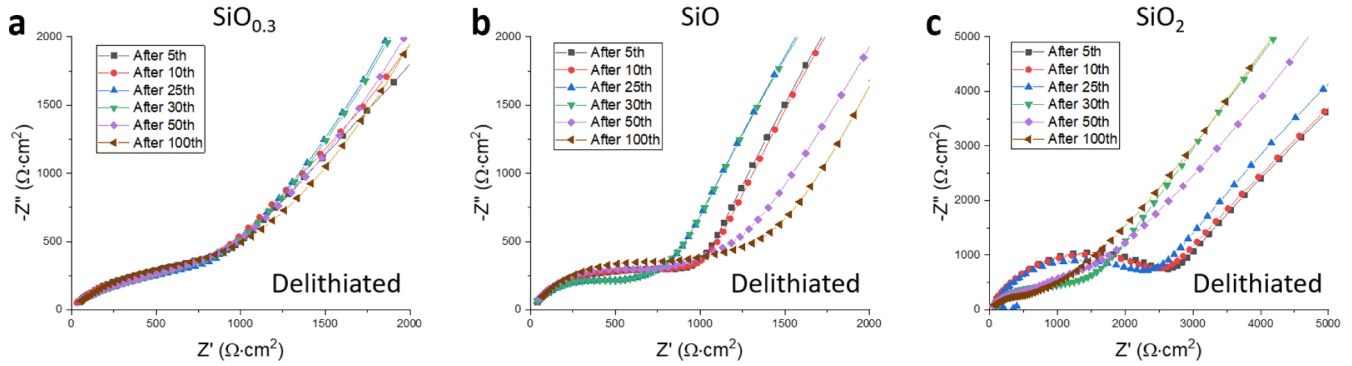

Figure 5. EIS spectra of fully delithiated (to 1.5 V) SiO_x films of (a) $SiO_{0.3}$, (b) SiO, and (c) SiO_2 thin-film electrodes over 100 cycles.

as the oxygen content increases, the peak 3 position appears at a higher voltage.[18] For the higher oxygen-content films in our study, peak 3 does indeed stabilize at a higher voltage with respect to the less oxygenated samples. The films with higher oxygen content also require an additional number of cycles before stabilizing at their respective positions. Moreover, for the SiO_2 thin-film electrode, it takes over 100 cycles before peak 3 reaches the higher voltage position.

It can be seen in Figure 4a that during the initial cycles, the peak 3 positions of films with higher oxygen content (e.g., SiO film) are at lower voltage positions compared to the $x = 0.3$ material. If these initial peak 3 shifts toward the higher voltage are solely due to structural changes, then the higher oxygenated samples should exhibit peak 3 positions at higher voltage positions starting from the initial cycles. In the early cycles, however, the SiO film's peak 3 position is at a lower voltage value than the films with lower x. This trend deviates from the expectations of structural change. It suggests that in the early cycles (1−20 cycles), peak 3 shifting is likely affected by kinetic factors such as impedance and overpotential that arise from higher concentrations of Si−O bonds that are more electrochemically resistive, although it may also relate to some differences in structures (i.e., stoichiometry) of lithium silicates formed during this reaction. In the later cycles, peak 3 of films with higher oxygen concentration (e.g., SiO sample) stabilizes at higher voltages than those of films with lower oxygen content. If impedance effects dominated in the later cycles, it would suggest that the SiO sample has a lower impedance than the $SiO_{0.3}$ films. However, SiO_x films with higher oxygen concentration generally exhibit higher impedance,[22] and hence, the differences in peak 3 positions after they stabilize are probably affected by structural differences. In particular, the difference likely reflects the structural differences in lithium silicate formation that result from various oxygen concentrations in the SiO_x, leading to the stabilization of lithium silicates with different compositions.

In the early cycles with higher-oxygen-content films, the larger number of cycles required to stabilize peak 3 is probably limited by diffusion. Higher concentrations of covalent Si−O bonds limit Li-ion's ability to break these bonds and diffuse, and the Li-ion solid-state diffusion is additionally hindered by the lower electron conduction in the presence of oxygen. The bonds present in highly concentrated films require subsequent cycling to break. It is likely that Si−O bonds are initially electrochemically inactive, and that Si−Si bonds established after lithiation can be reversibly cycled. This process, known as "electrochemical activation" of silica, is generally observed after additional cycling of SiO_2, resulting in an increase in ionic conductivity and capacity.[23−28] This activation of near-fully saturated films is observed in the current study. The CV curve in Figure 4b shows that the Li−Si peaks (peaks 1 and 2) start to emerge with subsequent cycling. During this period, the CV curve also shows an increased area under the curve, indicating an increase in capacity as more Li−Si species are activated. The additional capacity from activated Li−Si bonds is reflected in the discharge capacity versus cycle data seen in both Figures 2a and 4d, where gradual increases in capacity are observed after ∼15 cycles in the SiO_2 film.

3.3. EIS Measurements of SiO_x Films During Cycling. As shown in Section 3.1, the dQdV data suggests that increased oxygen content results in slower peak 3 stabilization during the initial cycles and that more cycles are required to stabilize this particular peak at higher voltage positions for films with higher oxygen content. This is likely related to the increased impedance of the films due to higher concentrations of Si−O bonds and their inherently insulating nature that impedes diffusion and bond breaking to form various lithium silicates.[24,25,27] To directly observe this impedance effect, EIS measurements were carried out every five cycles for each SiO_x film. From the spectra after full delithiation in Figure 5, it is generally seen that as oxygen content increases: (1) the overall resistance of each film increases, which can be seen by the size differences of the respective curves prior to their tails, and (2) as cycling proceeds, changes in both the size and the shapes of the spectra are more pronounced in films with higher oxygen content. The higher overall impedance observed in films with higher oxygen content is consistent with the peak 3 shifting differences observed in the previous section, where slower stabilization of peak 3 during the early cycles is attributed to kinetic factors rather than structural differences.

Furthermore, a dramatic change in the spectra is seen in SiO_2 in Figure 5c with a reduction in the overall resistance of the film from the 25th to 30th cycle, where activation occurs. Qualitatively, the middle-frequency semicircular region is reduced during the activation, suggesting that the charge-transfer properties at the interface between the surface of the film and the SEI are further enhanced during activation. The EIS measurements reveal the effects of various Si−O concentrations on the overall impedance experienced within the SiO_x films with additional cycling and that it is likely related to significant structural changes occurring with increasing oxygen content as shown in the evolution of dQdV peak shift in the later cycles.

3.4. XPS: Structural Changes in SiO_x Films during Electrochemical Cycling. The structural evolution of SiO_x thin-film electrodes during electrochemical cycling was

https://doi.org/10.1021/acsaem.2c01903
ACS Appl. Energy Mater. XXXX, XXX, XXX−XXX

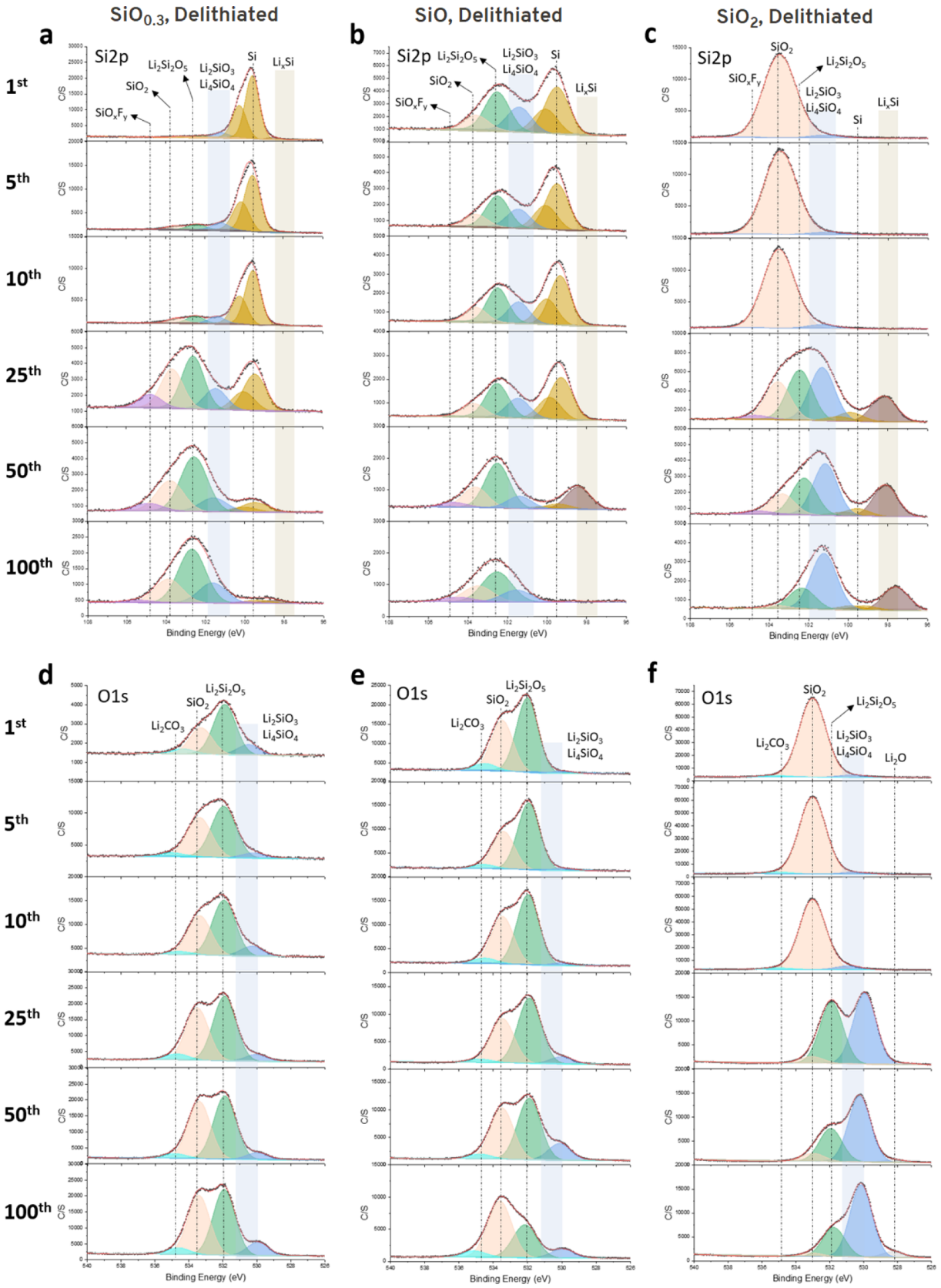

Figure 6. XPS profiles of Si 2p and O 1s spectra of delithiated (a,d) $SiO_{0.3}$, (b,e) SiO, and (c,f) SiO_2 thin-film electrodes after the 1st, 5th, 10th, 25th, 50th, and 100th cycles. All spectra were measured in the middle of the film after etching and then charge-corrected. This resulted in relatively high noise-to-signal ratios for carbon and near-surface-related spectra. The minor shift/mismatch of the peaks for a few of the spectra shown in Figure 6 (e.g., bulk Si peaks in the 10th and 25th vs 2nd and 5th cycles in Figure 6b) likely arises from small inaccuracies during the deconvolution of the C 1s C−C peaks for charge correction.

https://doi.org/10.1021/acsaem.2c01903
ACS Appl. Energy Mater. XXXX, XXX, XXX−XXX

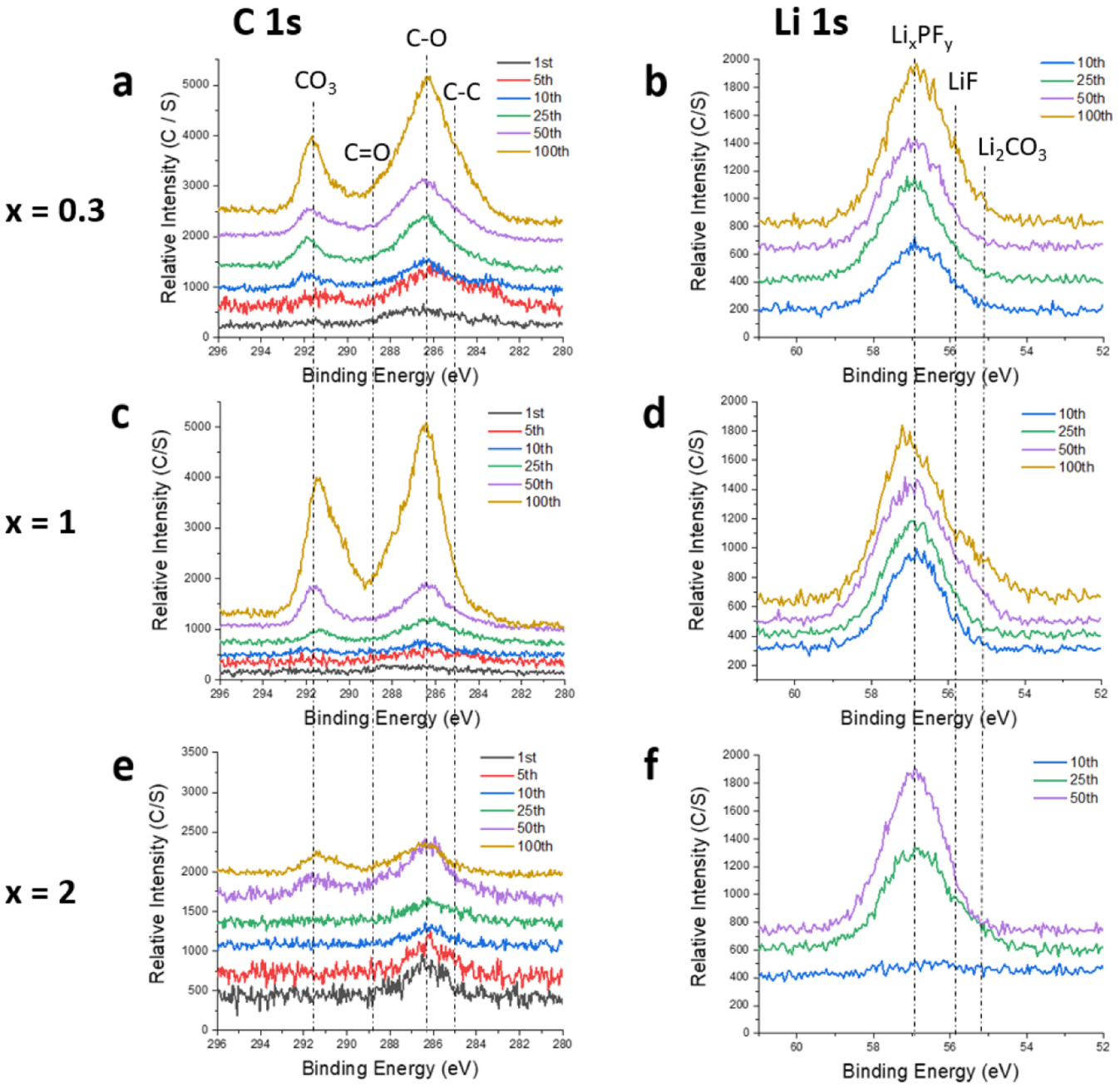

Figure 7. (a,c,e) XPS C 1s and (b,d,f) Li 1s spectra on the same samples discussed in the main text. Their respective peak positions are tabulated from the literature.

investigated using XPS measurements. Figure 6a–f shows the XPS spectra and respective fits for Si 2p and O 1s post delithiation after the 1st, 5th, 10th, 25th, 50th, and 100th cycles for each SiO_x thin film. Because the goal of this study is to look at chemical changes in the bulk of the film over subsequent cycling, XPS spectra after Ar-etching are shown. These measurements are all approximately at the center of the film, which was determined by the onset of Cu current collector peaks that indicated the point where the etch level had reached the bottom of the films. Examples of the full-depth profiles are shown in Figure S5, which show the Si 2p and Cu 2p depth profiles that were used to determine the approximate center position of the films. The spectra shown in Figure 6 hence reflect broader results in the middle of the film only. The fitted peaks in Figure 6 are color-coded in the following way: Si is light brown, Li_xSi is dark brown, Li_2SiO_3 and/or Li_4SiO_4 is blue, $Li_2Si_2O_5$ is green, SiO_2 is peach, SiO_xF_y is purple, Li_2CO_3 is sky-blue, and Li_2O is gray. Additionally, measured C 1s and Li 1s spectra in the middle of the film are partially inconclusive and are shown in Figure 7. The binding energy values of all relevant compositions are listed in Table S1.[29−37] The binding energy values of various Li_xSiO_y phases were determined in previous studies by either sol−gel or precipitation synthesis of Li_2SiO_3 and Li_4SiO_4[31] and crystallization of lithium disilicate glass at high temperature and pressure to create $Li_2Si_2O_5$ crystals.[38] It is important to note that the different Li_xSiO_y peaks fit in this study are an approximate way to interpret bonding distribution in the amorphous film. Thus, for the Li_2SiO_3 and Li_4SiO_4 peaks, a wider range of binding energy (100.5−102.1 eV) was used to fit these as an approximation.

https://doi.org/10.1021/acsaem.2c01903
ACS Appl. Energy Mater. XXXX, XXX, XXX−XXX

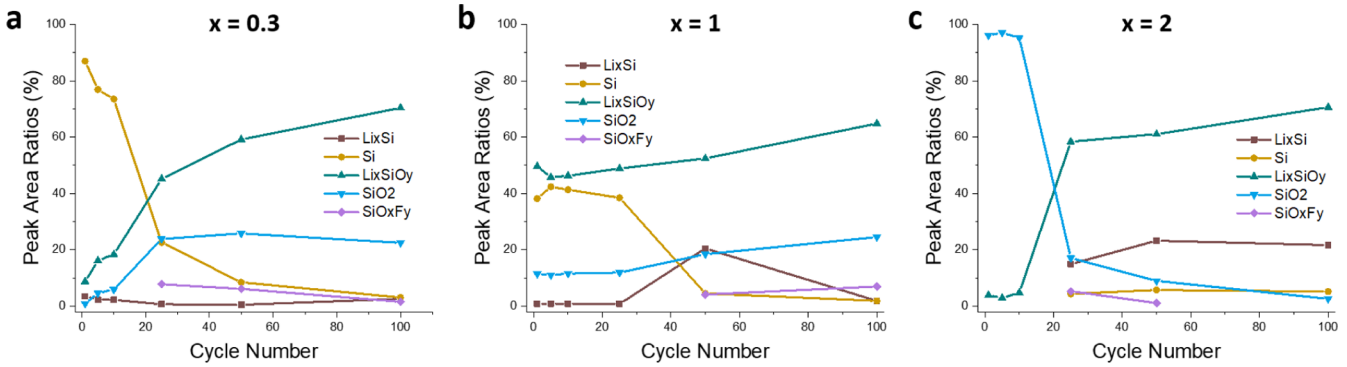

Figure 8. Ratios of fitted XPS Si 2p peak areas vs cycle number of the (a) $SiO_{0.3}$ film, (b) SiO film, and (c) SiO_2 film.

The summary of how these various peaks evolve during cycling is plotted in Figure 8, where the ratios of each of the peak's areas are plotted with evolving number of cycles.

3.4.1. $SiO_{0.3}$. After the first cycle, the Si 2p spectra in Figure 6a show that the film is primarily composed of bulk Si (99.4 eV) with minimal Li_xSiO_y and SiO_2 formation. The O 1s spectra after the first cycle show minimal intensity, which confirms the low detection of oxygen-related peaks within the bulk of the film. As cycling progresses, the Si 2p spectra show increased detection of oxygen-related peaks such as Li_2SiO_3 and/or Li_4SiO_4 (100.5−102.1 eV), $Li_2Si_2O_5$ (102.7 eV), and SiO_2 (103.5 eV) that are observed along with decreased intensities of bulk Si doublet peaks. The overall intensities of O 1s peaks are amplified as cycling continues, and these oxygen-related species are primarily composed of the following order throughout the 100 cycles: $Li_2Si_2O_5$, SiO_2, and Li_2SiO_3/Li_4SiO. By the 25th cycle, the Si 2p spectra show that the bulk Si peak has decreased, and oxygen-related peaks have increased significantly. This trend of decreasing bulk Si peaks and increasing oxygen-related peaks continues until the 100th cycle, where it shows almost negligible amounts of bulk Si peaks compared to the oxygen-related species mentioned above. By the 100th cycle, most of the reversible capacity is hence expected to arise from the lithium silicate species rather than from the lithiation/delithiation of pure Si.

In the $SiO_{0.3}$ electrode, the results in Figure 8a show that the film is gaining oxygen. This structural evolution also coincides with decreasing bulk Si−Si bonds. As cycling continues, the peak area ratio of bulk Si decays significantly as oxygen-related peaks including Li_xSiO_y and SiO_2 increase. It appears that the $SiO_{0.3}$ thin film reacts with oxygen from the liquid electrolyte since this is the only oxygen source present. This hypothesis is consistent with depth profiles of $SiO_{0.3}$ in Figure S5, which show higher intensities of oxygen-related peaks and lower concentrations of bulk Si near the surface. This gradient of oxygen-related phases' concentrations from the surface to the bottom of the electrodes indicates that the additional oxygen is being incorporated near the surface that is in contact with the liquid electrolyte.

3.4.2. SiO. During cycling, the Si 2p spectra evolution in Figure 6b shows that the SiO film's structural change is somewhat similar to the $SiO_{0.3}$ film. After the first cycle, initial Si−O bonds are converted to lithium silicates in addition to the remaining SiO_2. As cycling continues, Figure 8b shows that the SiO film also shows a reduction in bulk Si doublet peaks, while SiO_2 and Li_xSiO_y peaks grow during cycling. Note that the changes in peak area ratios in SiO are less pronounced than in the $SiO_{0.3}$ film, which suggests that starting with higher concentrations of oxygen within the film reduces the rate at which it drags oxygen from the excess oxygen source. By the 50th cycle, it can be seen in Si 2p spectra in Figure 8b that most of the bulk Si peaks have disappeared, although noticeable Li_xSi species were detected after the 50th cycle.

The SiO film shows similar structural change compared to $SiO_{0.3}$, where a reduction in bulk Si and addition of Si−O related species is generally observed with continued cycling but to a lesser extent. Additionally, a similar depth profile trend compared to $SiO_{0.3}$ film was observed in Figure S5c, where the SiO film shows higher concentrations of lithium silicates near the surface, supporting the idea that the oxygen is being dragged from the oxygen source near the surface (i.e., electrolyte).

3.4.3. SiO_2. The bonding changes that occur within SiO_2 during cycling are considerably different from the $SiO_{0.3}$ and SiO results, which is consistent with the substantial differences in the parallel electrochemical measurements in Figures 2a, 3, and 4d. As shown in the Si 2p spectra in Figure 6c (up to the 10th cycle), the film consists of largely SiO_2 with minimal growth of Li_2SiO_3/Li_4SiO_4 species. However, as activation begins around the 20th cycle, where bond-breaking and establishments of Si−Si bonds and are expected to occur,[23−27] the film undergoes significant structural rearrangement. This is seen in Figures 6c and 7c, where there is a significant reduction in the SiO_2 peak after the 25th cycle and a large growth of Li_xSiO_y species. As activation and cycling continue, both bulk Si and Li_xSi species are detected from the 25th to the 100th cycle, suggesting that some Si−Si bonds are established during activation after the breakage of Si−O bonds. This probably contributes to the observed increase in utilized capacity.

The initially dominant SiO_2 peak is minimal by the 100th cycle, and here the film is largely composed of Li_xSiO_y, Li_xSi, and small amounts of Si−Si. This observation differs substantially from the films with lower oxygen content where increased intensities of SiO_2 peak were observed. Instead, the SiO_2 films show a loss of SiO_2 throughout cycling. Recent investigation on the activation process of silica by Entwistle et al. showed direct evidence of the reduction of SiO_2 into amorphous silicon during the lithiation process.[24] This study further highlights the idea that the silica continues to reduce into other Si-related compounds such as Li_xSiO_y and bulk Si with additional cycling.

3.5. Cracking in the Films. As seen in Figure 6, small amounts of electrolyte-related components such as SiO_xF_y and Li_2CO_3 are detected at places that are close to the center of the films. This is likely to be related to the cracking caused by the large deformations that Si-based electrodes experience during

https://doi.org/10.1021/acsaem.2c01903
ACS Appl. Energy Mater. XXXX, XXX, XXX−XXX

cycling, which increases the available surface area for the electrolyte reaction and SEI formation. The SEM images of the top surfaces of the different films in Figure S6 show the extent of cracking that occurs. It is generally seen that as oxygen content increases, the film requires a larger number of cycles before cracks are observed. Cracks in the $SiO_{0.3}$ occur as early as the fifth cycle, whereas SiO films show no cracking until the 25th cycle. Moreover, the SiO_2 film did not show evidence of cracking until the 100th cycle as seen in Figure S6. This observation is also consistent with the concentrations of electrolyte-related species in the XPS measurements in Figures 6 and 8. The $SiO_{0.3}$ films that crack in earlier cycles show the SiO_xF_y peak as early as the 25th cycle, while the SiO and SiO_2 films with less cracking show this in later cycles, where the magnitudes of the SiO_xF_y and Li_2CO_3 peaks are also smaller compared to the $SiO_{0.3}$ material. Also, although cracking in the SiO_x films leads to more SEI formation, note that the crack spacings are larger than the film thickness. This implies that the amount of additional SEI formation due to cracking is a relatively small fraction of the total SEI present in most of the specimens, which is consistent with the observation that the electrolyte-related species generally show small contributions.

3.6. Oxygen Content Variations During Electrochemical Cycling. The evolving changes in Si, SiO_2, and Li_xSiO_y with subsequent cycling indicate that structural changes in the films vary with the initial amount of oxygen that is present. The significant increase in oxygen-related peaks and loss of Si in $SiO_{0.3}$ and SiO films, in addition to the loss of SiO_2 in SiO_2 films, suggest that different reaction mechanisms govern multiple structural changes that depend on the oxygen content of these films. Potential mechanisms are discussed in this section.

3.6.1. Oxygen Incorporation in $SiO_{0.3}$ and SiO Films. Figure 8a,b shows significantly increased detection in oxygen-related peaks, such as Li_xSiO_y and SiO_2, throughout cycling for both $SiO_{0.3}$ and SiO film. This suggests that oxygen is gained from the liquid electrolyte with subsequent cycling. It is difficult to speculate about the exact mechanism which causes the films to gain oxygen during cycling, but one possible explanation is that the oxygen is incorporated from the SEI (e.g., from reactions with Li_2CO_3 or Li_2O). Li_2O, a common SEI constituent, reacts with Si to form additional lithium silicate phases during electrochemical cycling.[33,39] Note here that the O 1s spectra in Figure 6 for all films in all cycled films do not show any evidence of Li_2O. This has been previously attributed to subsequent reactions between Li_2O and Si electrodes to form lithium silicate.[33] Negligible detection of the Li_2O peak in Figure 6 hence suggests that Li_2O formed on the surface of the electrode likely reacted with the bulk film, resulting in additional growth of lithium silicates with additional cycling that was observed in the XPS results. Additionally, for $SiO_{0.3}$ and SiO films, it can be seen in Figure 7a,c that as cycling progresses, there is a significant increase in the detection for both C−O and CO_3 bonds. This increasing concentration of organic compounds in the middle of the film could indicate that the films have more access to oxygen as cycling continues. Hence, other SEI-related compounds that build up throughout the film may be an additional source of oxygen for incorporation. Moreover, the increasing concentrations of these SEI-related species in the bulk of the film suggest that the thin-film SiO_x undergoes changes that effectively make the initial film material part of the SEI. This interpretation differs significantly from the traditional understanding of the SEI where the layer is formed directly on top of the electrode. The implication of this new finding is further discussed below.

Cracking may also increase the amount of SEI that is available for this reaction as it creates additional surface area. This is consistent with the fact that the $SiO_{0.3}$ film that showed cracking during as early as the fifth cycle in 14a exhibits the presence of the electrolyte-related SiO_xF_y peak earlier with larger intensities than samples with higher oxygen content that exhibit less cracking. It can also be seen that for $SiO_{0.3}$, a relatively sudden change in the XPS spectra is observed compared to the SiO film (e.g., changes from the 10th to 25th cycle in Figure 6a). This large and rapid change in the compositions of $SiO_{0.3}$ may be explained by the higher oxygen incorporation near the surface of the films evident in Figure S5. For $SiO_{0.3}$ in Figure S5a, the intensity gradient of the bulk Si peak is more apparent compared to that of SiO in Figure S5b. This likely results in a higher driving force for the oxygen incorporation reaction and could explain this sudden change compared to the results for SiO. The gain of oxygen during cycling for lower x films is also consistent with the peak 3 evolution of $SiO_{0.3}$ in Figures 3b and 4a, where the oxygen-related reaction peak 3 re-emerges after ∼60 cycles. In previous work with Si particles, XPS shows that the native oxide can react with lithium with further cycling to create additional Li_4SiO_4 and Li_2O phases.[30] In contrast, the results in Figure 6 suggest that oxygen incorporation originates from the liquid electrolyte, introducing low concentrations of oxygen in the SiO_x film throughout cycling. To our knowledge, this behavior has not been reported previously.

The rate at which the SiO film gains oxygen varies significantly compared to the $SiO_{0.3}$ film. The results in Figure 8b show that the structural changes in the SiO film are similar to the $SiO_{0.3}$ film, with increasing SiO_2 and Li_xSiO_y intensities as cycling continues. However, compared to the trends for the $SiO_{0.3}$ film shown in Figure 8a, the increases in the SiO_2 and Li_xSiO_y intensities in the SiO film are less pronounced than in $SiO_{0.3}$. This indicates that increasing the oxygen content reduces the rate of oxygen uptake.

3.6.2. Loss of Si−Si Bonds in the $SiO_{0.3}$ and SiO Film. In addition to the oxygen incorporation mentioned above, it can be seen in Figures 6a,b and 8a,b that there is a significant loss of pure Si−Si bonds with subsequent cycling for both the $SiO_{0.3}$ and SiO films. Possible explanations for the loss of Si may be attributed to (1) additional bonding of Si with oxygen that is incorporated from the electrolyte/SEI as mentioned above, (2) trapping of the Li_xSi species in the SEI layer, and (3) HF etching produced by hydrolysis of the $LiPF_6$ salt.

As mentioned previously, some Li_xSi was detected in the later cycles in both the $SiO_{0.3}$ and SiO films. Increases in the Li_xSi peak intensity were observed after 100 cycles in the $SiO_{0.3}$ and after 50 cycles in SiO. Fracture or delamination can lead to the trapping of some of the active material in the SEI, where it then becomes electrochemically inactive during subsequent cycling.[4,40]Figure S6b shows that the SiO film undergoes cracking around ∼25 cycles, and the Li_xSi species observed here is consistent with trapped Li_xSi within the SEI layer that forms along the cracks in the film. The presence of Li_xSi in films after full delithiation then suggests that this material is electrochemically inactive due to trapping in the insulating SEI, resulting in the loss of Si−Si. In the SiO film, significant Li_xSi was detected earlier (after 50 cycles). However, the amount of Li_xSi in the SiO film after 100 cycles shows negligible Li_xSi

https://doi.org/10.1021/acsaem.2c01903
ACS Appl. Energy Mater. XXXX, XXX, XXX−XXX

(i.e., significantly lower intensity than the $SiO_{0.3}$ film after 100 cycles). The mechanisms leading to Li_xSi after the 50th cycle in the SiO film are currently inconclusive, but it is possible that the higher oxygen content here leads to incomplete Li removal during delithiation.

In all samples, small amounts of SiO_xF_y peaks were identified in Figures 6 and 8 after the 25th cycle. These peaks also become more pronounced with additional cycling for the SiO film. The irreversible formation of SiO_xF_y generally occurs at the interface between the electrode and the SEI due to a reaction with HF formed from H_2O and the $LiPF_6$ salt. This can also result in some loss of active Si,[30,41] but these effects appear to be relatively small.

The XPS data for $SiO_{0.3}$ and SiO films in Figure 6a,b suggests that reversible-capacity contribution from pure Si should be minimal after a large number of cycles, as shown by the negligible detection of bulk Si after a large number of cycles (after the 50th cycle). In addition to deformation-induced capacity loss, the loss of Si−Si bonding from the formation of oxygen-related species that are either electronically insulating (SiO_2) or irreversible (Li_4SiO_4 and Li_2O) likely contributes to the rapid capacity degradation of $SiO_{0.3}$, as seen in Figure 2a.[5,7] However, it is also worth noting that the EIS spectra show minimal change for $SiO_{0.3}$ throughout cycling (Figure 5a), which indicates that the Li-ion conductivity does not change even after significant increases in these oxygen-related species. Previous XPS studies with SiO_x generally consist of measurements during or after a single lithiation/delithiation sequence where the pre-existing and prominent bulk Si peak still remains as a dominant contribution to the spectra.[30−34] Based on the results for $SiO_{0.3}$ and SiO films after 50 and 100 cycles where little to no Si peak is observed, the loss of Si−Si bonds is a significant factor in the structural evolution of SiO_x thin films after repeated electrochemical cycling.

3.6.3. Disproportionation of SiO_2. In the SiO_2 films, the evolution of the Si, SiO_2, and Li_xSiO_y peaks during cycling differs considerably from the $SiO_{0.3}$ and SiO films. Here, Figure 8c shows the rapid decay of SiO_2 intensities as activation continues. The corresponding increase in Li_xSiO_y and minor amounts of Si−Si bonding after a large number of cycles indicates that silica disproportionates to form Li_xSiO_y and Si−Si, which is consistent with previous studies.[23,25,28,36] This is described by

$$5SiO_2 + 4Li^+ + 4e^- \leftrightarrows 2Li_2Si_2O_5 + Si \quad (1)$$

$$2SiO_2 + 4Li^+ + 4e^- \leftrightarrows Li_4SiO_4 + Si \quad (2)$$

$$SiO_2 + 4Li^+ + 4e^- \leftrightarrows 2Li_2O + Si \quad (3)$$

The additional free Si here can then contribute to the additional capacity, which is observed after activation in Figures 2a and 4d. It has also been shown that the reduction of SiO_2 via lithium insertion results in a positive feedback loop, where increased electronic conductivity from newly formed silicate species further facilitates the reduction of SiO_2 with continuous cycling.[24] This continuous reduction process can explain the observed structural change in Figures 6c and 8c with the rapid decay of SiO_2 intensities after activation and a corresponding increase in capacity. Equation 2 provides a convenient basis for estimating the amount of free Si based on the assumption that all of the oxygen in SiO_2 is irreversibly converted to Li_4SiO_4. The free Si here corresponds to half of the total amount in the initial SiO_2 film, such that converting all of the oxygen to Li_4SiO_4 corresponds to a total capacity increase of ~1800 mA h/g_{Si}. Figure 2a shows a lower capacity increase (up to ~450 mA h/g_{Si}) after activation, which implies that the SiO_2 does not fully disproportionate via eq 2.

3.7. Correlations between XPS and Electrochemical Data. The variations in the lithium silicate peaks that evolve during the initial 25 cycles for different SiO_x films can also be correlated with the oxygen-related peak in the dQdV data in Figure 4a. As noted in section 3.1, the normalized CV curves (e.g., Figure S3) show increased lithium uptake during the reaction represented by peak 3 (i.e., lithium silicate formation). Based on these data, films with higher oxygen content are expected to grow more lithium silicate species during this reaction. This is supported in the XPS measurements in Figure 8, where the relative amount of lithium silicate present varies significantly in the $SiO_{0.3}$ and SiO films during the first 25 cycles. A larger silicate peak contribution in the SiO film compared to the $SiO_{0.3}$ film shows that there is increased lithium uptake, and this is also correlated with the silicate peak in the normalized CV curves in Figure S3. Furthermore, different positions of stabilized peak 3 for all films after the initial cycles suggest that the lithium silicate compositions vary with the initial oxygen content. Although exact lithium silicate compositions are difficult to probe in amorphous films, varying intensity ratios between the $Li_2Si_2O_5$ and Li_2SiO_3/Li_4SiO_4 peaks in Figure 8 for different samples are consistent with the idea that lithium silicate compositions vary with oxygen content. Overall, the correlations between XPS and electrochemical data strongly support the idea that peak 3 in the dQdV analysis is closely related to lithium silicate formation.

The voltage hysteresis that is commonly observed in Si-based electrodes has been attributed to differences in the atomic bonding structure in these materials during lithiation versus delithiation.[48] Films with different initial oxygen contents also exhibit this type of voltage hysteresis, as seen in the voltage versus normalized capacity data in Figure 4c. This implies that the material with the same Li content exhibits structural differences (i.e., different Si−O−Li bonding configurations) when it is formed during lithiation or delithiation. In thin films, elastic strain energy in the electrode also contributes to voltage hysteresis, but this only accounts for roughly 60 mV (i.e., less than half of the amount measured).[42] Electrodes also exhibit larger hysteresis at higher currents due to higher overpotential.[43−46] However, in Si thin-film electrodes, these overpotential effects are small at the low current densities used for the experiments in Fig. 4;[45,47] hence, the kinetic contributions are expected to be minimal here (especially for films with low x). Thus, while kinetic factors make some contribution to the voltage hysteresis of the highly oxygenated films during the initial cycles, the later cycles show trends that are consistent with structural differences in films. These differences are also reflected in the different peak 3 positions in Figure 4a. Hence, the large voltage hysteresis in the later cycles is mainly attributed to structural bonding differences in the material that varies with the lithiation/delithiation history. In other words, the differences reflected in the voltage hysteresis here mean that amorphous films with the same composition [i.e., the same state of charge (SOC)] have a significantly different atomic structure during the lithiation versus delithiation sequence. In Figure 4c, with increasing oxygen content in the film, increased hysteresis is observed, which suggests that higher oxygen concentrations result in

https://doi.org/10.1021/acsaem.2c01903
ACS Appl. Energy Mater. XXXX, XXX, XXX−XXX

larger structural differences. This is also consistent with the observation with the XPS measurements that the films with lower oxygen content gain oxygen with additional cycling as increasing hysteresis magnitudes are shown in Figure 4d for $SiO_{0.3}$, $SiO_{0.5}$, and SiO films after 15−20 cycles as the cycles proceed.

The SiO_2 films show a very different hysteresis behavior compared to the films with less oxygen. Voltage hysteresis at 50% SOC defined by the normalized capacities of each film during 100 cycles is plotted in the bottom figure of Figure 4d. For a SiO_x film composition $x < 1$, it is generally seen that at least for the first half of 100 cycles, the films show increased hysteresis with increasing oxygen content, with a slight dip in the values for ∼20 cycles or less and then a gradual increase in the value until the end of 100th cycle. However, the hysteresis behavior of the SiO_2 film shows almost the opposite trend from the others. For the initial 20 cycles, SiO_2 not only exhibits much larger hysteresis but also shows an initial increase in the hysteresis value during the first 20 cycles. Around ∼20 cycles, there is a dramatic decrease in the hysteresis of SiO_2 film as the activation of silica and the increase in capacity is observed. With increasing Li_xSiO_y and Si peaks that result from the breakage of initial Si−O bonds via disproportionation reactions discussed above in Section 4.1.3, the decrease in hysteresis during activation in Figure 4d suggests that the structural disproportionation of SiO_2 reflects their hysteresis behaviors throughout cycling.

The close overlap of the normalized voltage profiles during lithiation in Figure 4c suggests that most of the reversible Li ions are stored in remarkably similar local bonding environments for different SiO_x films. Minor detection of Si−Si bonds in the later cycles of all samples in Figure 6 then suggests that similar local bonding configurations where Li can be reversibly inserted and extracted likely have some amount of oxygen. This differs substantially from previous arguments that most lithium silicate species are irreversible. It should be noted that given the amorphous nature of these films, it is difficult to ascertain how much oxygen is involved in the bonding configurations that lead to reversible cycling.

The differences in the SiO_x film composition primarily affect the voltage hysteresis during delithiation. This suggests that higher oxygen levels correspond to an increase in the difficulty of removing Li ions. During delithiation, the Si structure undergoes significant structural relaxation;[48] thus, the variations seen with different SiO_x materials imply that Si−O bonding affects how the overall film relaxes during lithium removal. The differences in the relaxation behavior during delithiation may also reflect the behavior of inactive components (i.e., Li_4SiO_4 and SiO_2) in the cycled films.

3.8. Evolution toward Equilibrated Compositions. In Figure 8, the Li_xSiO_y, SiO_2, and bulk Si in all SiO_x films show similar peak area ratios after the 25th cycle, with subsequent evolution toward similar compositions. The quantitative similarity for all phases in the $SiO_{0.3}$ and SiO films is particularly striking. Furthermore, the discharge capacities in Figure 2a show that by the 100th cycle, the utilized capacity reaches similar values of roughly 1000 mA h/g for all films. This observation of similar capacities and the amounts of each species present after a large number of cycles suggests that SiO_x thin films undergo structural changes where the continued lithium insertion and removal leads to film structures with similar structures and compositions. Two likely mechanisms that result in these similar states are described above: (1) some oxygen is incorporated from the liquid electrolyte in the $SiO_{0.3}$ and SiO films, possibly via reactions with the SEI, and (2) disproportionation/reduction converts the oxygen-rich material into various lithium silicate species and disproportionated Si.[26,27] This hypothesis is strongly supported by the experiments with the lower oxygen content films ($SiO_{0.3}$ and SiO), whereas there are some quantitative differences between these data sets and the lithium silicate content for the SiO_2 material. This may indicate that the higher oxygen content alters the silicate formation kinetics; however, the similar reversible capacities after 100 cycles still suggest that all of the materials are approaching a similar state. While the reaction sequences discussed above are speculative at this point, this work indicates that the solid solution behavior of SiO_x films changes significantly during cycling.

It is also worth noting that the cracking effects in the SiO_x films investigated here are potentially relevant to SEI cracking on particles. Although the mechanical constraints are different in the current thin film study, the observation that oxygen content has a substantial effect on film cracking may affect phenomena near particle surfaces as well (i.e., as cracks may facilitate the addition of oxygen-related reactions with an additional surface area of exposed electrodes created within the films). The potential impact of this cracking is particularly relevant, in light of the conclusion that the Si−O reactivity causes the near-surface portion of the SiO_x electrode material to effectively become part of the SEI. However, a systematic study of the effects of different cracking behaviors as a function of electrode oxygen content (i.e., chemo-mechanical effects) would require a broader investigation where the crack spacing can be independently varied. Lastly, the overall results from our experiments suggest that using higher-oxygen-content SiO_x ($1 < x < 2$) as a surface layer may provide a better performance, with structural stabilization occurring in shorter times while also limiting the mechanical damage of the surface film.

4. CONCLUSIONS

The effect of the oxygen content of SiO_x thin-film electrodes on both electrochemical and structural changes was investigated. This study used thinner films (∼50 nm) than prior work, which made it possible to focus on phenomena near the surface. The chemical changes and their relationship to the initial oxygen content were investigated with a variety of methods. In general, the films exhibited decreased capacity as the oxygen content increased. More importantly, the evolution of the oxygen-related $dQd\mathit{V}$ peak showed that with increased Si−O bonding, longer cycling is required to stabilize the structure. The EIS data further highlights that higher concentrations of Si−O bonds correspond to slower kinetics, such that more time/cycling is required to restructure bonding during early cycles. Based on XPS and other measurements, two main oxygen-related mechanisms were observed: (1) oxygen incorporation from the electrolyte leads to the loss of Si−Si bonds and an increase in Si−O bonding in films with composition $SiO_{0.3}$ and SiO, and (2) significant reduction/disproportionation of SiO_2 occurs in highly oxygenated SiO_2 films (i.e., leading to increased concentrations of Li_xSiO_y and Si−Si). Although the changes that occur vary with the initial Si−O composition, by the end of the 100th cycle, all of the films exhibit similar capacities and have chemical compositions that are qualitatively similar. This suggests that reactions with the electrolyte and Li can modify the film composition in

https://doi.org/10.1021/acsaem.2c01903
ACS Appl. Energy Mater. XXXX, XXX, XXX−XXX

similar ways, regardless of the initial SiO_x composition. This outcome likely arises from similarities in the operative reaction mechanisms and suggests that surface layers will consist of equilibrated Si−O−Li chemistries after long-term cycling.

The large changes observed in the 50 nm thin films in this study imply that Si and SiO_x particle-based electrode materials will undergo similar irreversible changes in surface layers that are at least tens of nanometers thick, effectively causing these regions to become part of the SEI passivating layer. This is distinctly different from the common view of the SEI as a surface layer that forms on top of the active material. The oxygen incorporation highlighted in the $SiO_{0.3}$ and SiO thin films is evidence of direct reactions with the electrolyte and/or the SEI. The additional disproportionation mechanism observed with the SiO_2 film is also particularly relevant because this composition is similar to the surface oxide on most Si/SiO_x particles. This understanding suggests that SEI films can be engineered by controlling the oxygen content of the surface regions in both Si- and SiO_x -based electrodes, where the different types of reactions observed for various films in this study can provide useful guidelines for creating surface passivating layers with improved properties.

■ ASSOCIATED CONTENT

Supporting Information

The Supporting Information is available free of charge at https://pubs.acs.org/doi/10.1021/acsaem.2c01903.

Additional results, SEM images, electrochemical data, and XPS (PDF)

■ AUTHOR INFORMATION

Corresponding Authors

Jung Hwi Cho − *School of Engineering, Brown University, Providence, Rhode Island 02912, United States*; Email: jung_hwi_cho@brown.edu

Brian W. Sheldon − *School of Engineering, Brown University, Providence, Rhode Island 02912, United States*; orcid.org/0000-0002-9593-891X; Email: brian_sheldon@brown.edu

Authors

Xingcheng Xiao − *Chemical and Materials Systems Laboratory, General Motors Research and Development Center, Warren, Michigan 48090, United States*; orcid.org/0000-0002-0138-059X

Mark W. Verbrugge − *Chemical and Materials Systems Laboratory, General Motors Research and Development Center, Warren, Michigan 48090, United States*

Complete contact information is available at: https://pubs.acs.org/10.1021/acsaem.2c01903

Author Contributions

J.C., X.X., M.W.V, and B.W.S. discussed the design of the experiments. J.C. conducted all relevant experiments and analysis. J.C., X.X., M.W.V, and B.W.S. contributed to writing the paper.

Notes

The authors declare no competing financial interest.

■ ACKNOWLEDGMENTS

The authors acknowledge research support from General Motors and the National Science Foundation (DMR-1832829).

■ REFERENCES

(1) Jiao, M.; Wang, Y.; Ye, C.; Wang, C.; Zhang, W.; Liang, C. High-capacity SiO (0≤x≤2) as promising anode materials for next-generation lithium-ion batteries. *J. Alloys Compd.* **2020**, *842*, 155774.

(2) Zeng, X.; Li, M.; Abd El-Hady, D.; Alshitari, W.; Al-Bogami, A. S.; Lu, J.; Amine, K. Commercialization of Lithium Battery Technologies for Electric Vehicles. *Adv. Energy Mater.* **2019**, *9*, 1900161.

(3) Blomgren, G. E. The Development and Future of Lithium Ion Batteries. *J. Electrochem. Soc.* **2016**, *164*, A5019−A5025.

(4) Takezawa, H.; Iwamoto, K.; Ito, S.; Yoshizawa, H. Electrochemical behaviors of nonstoichiometric silicon suboxides (SiOx) film prepared by reactive evaporation for lithium rechargeable batteries. *J. Power Sources* **2013**, *244*, 149−157.

(5) Haruta, M.; Doi, T.; Inaba, M. Oxygen-Content Dependence of Cycle Performance and Morphology Changes in Amorphous-SiOx Thin-Film Negative Electrodes for Lithium-Ion Batteries. *J. Electrochem. Soc.* **2019**, *166*, A258−A263.

(6) Nguyen, C. C.; Choi, H.; Song, S.-W. Roles of Oxygen and Interfacial Stabilization in Enhancing the Cycling Ability of Silicon Oxide Anodes for Rechargeable Lithium Batteries. *J. Electrochem. Soc.* **2013**, *160*, A906−A914.

(7) Hsu, C.-H.; Chen, H.-Y.; Tsai, C.-J. Stoichiometry dependence of electrochemical behavior of silicon oxide thin film for lithium ion batteries. *J. Power Sources* **2019**, *438*, 226943.

(8) Li, Z.; Jin, J.; Yuan, Z.; Yang, W. Surface modification of SiOx film anodes by laser annealing and improvement of cyclability for lithium-ion batteries. *Mater. Sci. Semicond. Process.* **2021**, *121*, 105300.

(9) Choi, I.; Lee, M. J.; Oh, S. M.; Kim, J. J. Fading mechanisms of carbon-coated and disproportionated Si/SiO negative electrode (Si/SiO /C) in Li-ion secondary batteries: Dynamics and component analysis by TEM. *Electrochim. Acta* **2012**, *85*, 369−376.

(10) Hsiao, C.-Y.; Shih, C.-F.; Su, K.-W.; Chen, H.-J.; Fu, S.-W. Self-assembled Si/SiO2 superlattice in Si-rich oxide films. *Appl. Phys. Lett.* **2011**, *99*, 053115.

(11) Thompson, N. L.; Alamdari, S.; Hsu, C.-W.; Williamson, G. A.; Holmberg, V. C. DiffCapAnalyzer A Python Package for Quantitative Analysis of Total Differential Capacity Data. *J. Open Source Software* **2020**, *5*, 2624.

(12) Molinari, M.; Rinnert, H.; Vergnat, M. Visible photoluminescence in amorphous SiOx thin films prepared by silicon evaporation under a molecular oxygen atmosphere. *Appl. Phys. Lett.* **2003**, *82*, 3877−3879.

(13) Alfonsetti, R.; Lozzi, L.; Passacantando, M.; Picozzi, P.; Santucci, S. XPS studies on SiOx thin films. *Appl. Surf. Sci.* **1993**, *70-71*, 222−225.

(14) Bourderau, S.; Brousse, T.; Schleich, D. M. Amorphous silicon as a possible anode material for Li-ion batteries. *J. Power Sources* **1999**, *81-82*, 233−236.

(15) Obrovac, M. N.; Christensen, L. Structural Changes in Silicon Anodes during Lithium Insertion/Extraction. *Electrochem. Solid-State Lett.* **2004**, *7*, A93.

(16) Wang, J. W.; He, Y.; Fan, F.; Liu, X. H.; Xia, S.; Liu, Y.; Harris, C. T.; Li, H.; Huang, J. Y.; Mao, S. X.; Zhu, T. Two-Phase Electrochemical Lithiation in Amorphous Silicon. *Nano Lett.* **2013**, *13*, 709−715.

(17) Wen, C. J.; Huggins, R. A. Chemical diffusion in intermediate phases in the lithium-silicon system. *J. Solid State Chem.* **1981**, *37*, 271−278.

(18) Al-Maghrabi, M. A.; Suzuki, J.; Sanderson, R. J.; Chevrier, V. L.; Dunlap, R. A.; Dahn, J. R. Combinatorial Studies of Si1−xOxas a Potential Negative Electrode Material for Li-Ion Battery Applications. *J. Electrochem. Soc.* **2013**, *160*, A1587−A1593.

(19) Zeng, J.; Liu, Q.; Jia, D.; Liu, R.; Liu, S.; Zheng, B.; Zhu, Y.; Fu, R.; Wu, D. A polymer brush-based robust and flexible single-ion conducting artificial SEI film for fast charging lithium metal batteries. *Energy Storage Mater.* **2021**, *41*, 697−702.
(20) Yu, B.-C.; Hwa, Y.; Park, C.-M.; Sohn, H.-J. Reaction mechanism and enhancement of cyclability of SiO anodes by surface etching with NaOH for Li-ion batteries. *J. Mater. Chem. A* **2013**, *1*, 4820−4825.
(21) Lei, X.; Wang, J.; Huang, K. Fast Li-Ion Transport in Amorphous Li2Si2O5: An Ab Initio Molecular Dynamics Simulation. *J. Electrochem. Soc.* **2016**, *163*, A1401−A1407.
(22) Meng, X.; Huo, H.; Cui, Z.; Guo, X.; Dong, S. Influences of oxygen content on the electrochemical performance of a-SiOx thin-film anodes. *Electrochim. Acta* **2018**, *283*, 183−189.
(23) Verners, S. A.; Simone, A. Characterization of the structural response of a lithiated SiO2 / Si interface: A reactive molecular dynamics study. *Mech. Mater.* **2019**, *136*, 103030.
(24) Entwistle, J. E.; Booth, S. G.; Keeble, D. S.; Ayub, F.; Yan, M.; Corr, S. A.; Cumming, D. J.; Patwardhan, S. V. Insights into the Electrochemical Reduction Products and Processes in Silica Anodes for Next-Generation Lithium-Ion Batteries. *Adv. Energy Mater.* **2020**, *10*, 2001826.
(25) Sivonxay, E.; Aykol, M.; Persson, K. A. The lithiation process and Li diffusion in amorphous SiO2 and Si from first-principles. *Electrochim. Acta* **2020**, *331*, 135344.
(26) Renman, V.; Blanco, M. V.; Norberg, A. N.; Vullum-Bruer, F.; Svensson, A. M. Electrochemical activation of a diatom-derived SiO2/C composite anode and its implementation in a lithium ion battery. *Solid State Ionics* **2021**, *371*, 115766.
(27) Lepoivre, F.; Larcher, D.; Tarascon, J.-M. Electrochemical Activation of Silica for Enhanced Performances of Si-Based Electrodes. *J. Electrochem. Soc.* **2016**, *163*, A2791−A2796.
(28) Ban, C.; Kappes, B. B.; Xu, Q.; Engtrakul, C.; Ciobanu, C. V.; Dillon, A. C.; Zhao, Y. Lithiation of silica through partial reduction. *Appl. Phys. Lett.* **2012**, *100*, 243905.
(29) Philippe, B.; Hahlin, M.; Edström, K.; Gustafsson, T.; Siegbahn, H.; Rensmo, H. Photoelectron Spectroscopy for Lithium Battery Interface Studies. *J. Electrochem. Soc.* **2015**, *163*, A178−A191.
(30) Philippe, B.; Dedryvère, R.; Gorgoi, M.; Rensmo, H.; Gonbeau, D.; Edström, K. Improved Performances of Nanosilicon Electrodes Using the Salt LiFSI: A Photoelectron Spectroscopy Study. *J. Am. Chem. Soc.* **2013**, *135*, 9829−9842.
(31) Philippe, B.; Dedryvère, R.; Allouche, J.; Lindgren, F.; Gorgoi, M.; Rensmo, H.; Gonbeau, D.; Edström, K. Nanosilicon Electrodes for Lithium-Ion Batteries: Interfacial Mechanisms Studied by Hard and Soft X-ray Photoelectron Spectroscopy. *Chem. Mater.* **2012**, *24*, 1107−1115.
(32) Cao, C.; Abate, I. I.; Sivonxay, E.; Shyam, B.; Jia, C.; Moritz, B.; Devereaux, T. P.; Persson, K. A.; Steinrück, H.-G.; Toney, M. F. Solid Electrolyte Interphase on Native Oxide-Terminated Silicon Anodes for Li-Ion Batteries. *Joule* **2019**, *3*, 762−781.
(33) Radvanyi, E.; De Vito, E.; Porcher, W.; Jouanneau Si Larbi, S. An XPS/AES comparative study of the surface behaviour of nano-silicon anodes for Li-ion batteries. *J. Anal. At. Spectrom.* **2014**, *29*, 1120−1131.
(34) Coyle, J. E.; Brumbach, M. T.; Veith, G. M.; Apblett, C. A. Investigating the Chemical Reactivity of Lithium Silicate Model SEI Layers. *J. Phys. Chem. C* **2020**, *124*, 8153−8161.
(35) Philippe, B.; Dedryvère, R.; Gorgoi, M.; Rensmo, H.; Gonbeau, D.; Edström, K. Role of the LiPF6 Salt for the Long-Term Stability of Silicon Electrodes in Li-Ion Batteries - A Photoelectron Spectroscopy Study. *Chem. Mater.* **2013**, *25*, 394−404.
(36) Yan, N.; Wang, F.; Zhong, H.; Li, Y.; Wang, Y.; Hu, L.; Chen, Q. Hollow Porous SiO2 Nanocubes Towards High-performance Anodes for Lithium-ion Batteries. *Sci. Rep.* **2013**, *3*, 1568.
(37) Wood, K. N.; Teeter, G. XPS on Li-Battery-Related Compounds: Analysis of Inorganic SEI Phases and a Methodology for Charge Correction. *ACS Appl. Energy Mater.* **2018**, *1*, 4493−4504.
(38) Buchner, S.; Radtke, C.; Balzaretti, N. M. Densification of Lithium Disilicate under High Pressure Investigated by XPS. *Open J. Inorg. Non-Metallic Mater.* **2013**, *03*, 15−21.
(39) Schroder, K. W.; Dylla, A. G.; Harris, S. J.; Webb, L. J.; Stevenson, K. J. Role of Surface Oxides in the Formation of Solid-Electrolyte Interphases at Silicon Electrodes for Lithium-Ion Batteries. *ACS Appl. Mater. Interfaces* **2014**, *6*, 21510−21524.
(40) Bao, W.; Fang, C.; Cheng, D.; Zhang, Y.; Lu, B.; Tan, D. H. S.; Shimizu, R.; Sreenarayanan, B.; Bai, S.; Li, W.; Zhang, M.; Meng, Y. S. Quantifying lithium loss in amorphous silicon thin-film anodes via titration-gas chromatography. *Cell Rep. Phys. Sci.* **2021**, *2*, 100597.
(41) Shi, F.; Ross, P. N.; Somorjai, G. A.; Komvopoulos, K. The Chemistry of Electrolyte Reduction on Silicon Electrodes Revealed by in Situ ATR-FTIR Spectroscopy. *J. Phys. Chem. C* **2017**, *121*, 14476−14483.
(42) Sheldon, B. W.; Soni, S. K.; Xiao, X.; Qi, Y. Publisher's Note: Stress Contributions to Solution Thermodynamics in Li-Si Alloys [Electrochem. Solid-State Lett., 15, A9 (2012)]. *Electrochem. Solid-State Lett.* **20122012**, *15*, S3.
(43) Song, Y. C.; Soh, A. K.; Zhang, J. Q. On stress-induced voltage hysteresis in lithium ion batteries: impacts of material property, charge rate and particle size. *J. Mater. Sci.* **2016**, *51*, 9902−9911.
(44) Jiang, Y.; Offer, G.; Jiang, J.; Marinescu, M.; Wang, H. Voltage Hysteresis Model for Silicon Electrodes for Lithium Ion Batteries, Including Multi-Step Phase Transformations, Crystallization and Amorphization. *J. Electrochem. Soc.* **2020**, *167*, 130533.
(45) Jagannathan, M.; Chandran, K. S. R. Analytical modeling and simulation of electrochemical charge/discharge behavior of Si thin film negative electrodes in Li-ion cells. *J. Power Sources* **2014**, *247*, 667−675.
(46) Nitta, N.; Yushin, G. High-Capacity Anode Materials for Lithium-Ion Batteries: Choice of Elements and Structures for Active Particles. *Part. Part. Syst. Charact.* **2014**, *31*, 317−336.
(47) Baker, D. R.; Verbrugge, M. W.; Xiao, X. An approach to characterize and clarify hysteresis phenomena of lithium-silicon electrodes. *J. Appl. Phys.* **2017**, *122*, 165102.
(48) Kim, K. J.; Wortman, J.; Kim, S.-Y.; Qi, Y. Atomistic Simulation Derived Insight on the Irreversible Structural Changes of Si Electrode during Fast and Slow Delithiation. *Nano Lett.* **2017**, *17*, 4330−4338.

https://doi.org/10.1021/acsaem.2c01903
ACS Appl. Energy Mater. XXXX, XXX, XXX−XXX